Final Technical Report

USGS Award 06HQGR0025

"ANOTHER LOOK AT THE 1906 SAN FRANCISCO EARTHQUAKE"

P.I. Gregory C. Beroza
Department of Geophysics
397 Panama Mall
Stanford, CA, 94305-2215

Phone: (650) 723-4958
Fax: (650) 725-7344
Email: Beroza@stanford.edu

Research supported by the U.S. Geological Survey (USGS), Department of the Interior, under USGS award number 06-HQ-GR-0025. The views and conclusions contained in this document are those of the authors and should not be interpreted as necessarily representing the official policies, either expressed or implied, of the U.S. Government.

Technical Abstract

We reconcile two previously discordant source models of the 1906 San Francisco earthquake and obtain a model that satisfies both triangulation and seismic data by allowing the rupture velocity to exceed the shear-wave velocity. Employing a projection method to remove the dependence on initial station positions allowed us to make use of a more stable triangulation network, including nonrepeated angle observations along the northern San Andreas fault. This strengthens the case for significant slip over the entire northern segment of the San Andreas fault from San Juan Bautista to Cape Mendocino during the 1906 earthquake. We also found that the teleseismic body-wave data can be reconciled with the geodetically derived slip model by allowing supershear rupture. This resolves a longstanding conflict between the two previous slip models (geodetic and seismic) of this earthquake. Supershear rupture has long been recognized as a theoretical possibility for strike-slip faulting, and it has been observed in several recent large strike-slip earthquakes, which raises the prospect that it might be typical for such events. Supershear rupture leads to substantially different strong ground motion, and as a result, may need to be taken into account when developing ground motion prediction relations for large strike-slip earthquakes. Our final slip model has a seismic moment of 7.9×10^{20} N m, which corresponds to a moment magnitude of M_w 7.9

Publications resulting from this grant include:

2008 Aagaard, B. T., and G. C. Beroza, The 1906 San Francisco earthquake a century later: introduction to the special section, *Bull. Seismol. Soc. Am.* (in press).

2008 Song, S. G., G. C. Beroza, and P. Segall, A Unified Source Model for the 1906 San Francisco Earthquake, *Bull. Seismol. Soc. Am.,* (in press).

Award # 06-HQ-GR-0025
Another Look at the 1906 San Francisco Earthquake

Gregory C. Beroza
Department of Geophysics
397 Panama Mall
Stanford, CA, 94305-2215

Phone: (650) 723-4958
Fax: (650) 725-7344
beroza@geo.stanford.edu

Non-Technical Abstract

We reconcile previously contradictory models of the 1906 earthquake rupture – one based on geodetic data and one based on seismological data. Our unified model demonstrates that the 1906 earthquake ruptured approximately 300 miles of the San Andreas Fault, and that the magnitude of the earthquake was 7.9. The velocity of rupture in the earthquake to the north of San Francisco exceeded the shear wave velocity of the Earth's crust. Such "super-shear" rupture has a strong effect on strong ground shaking, may explain some aspects of shaking in 1906, and should be taken into account in future earthquake hazard forecasts for large strike-slip earthquakes.

Another Look at the 1906 San Francisco Earthquake

Two previous source models of the 1906 earthquake, one based on geodetic data (Thatcher *et al*., 1997) and the other based on seismic data (Wald *et al*., 1993), differ from one another, particularly in the total rupture length. The geodetic model maps slip from San Juan Bautista to Cape Mendocino (~500 km); whereas, the seismic model finds almost no slip north of Point Arena (~300 km). We can reconcile these models if the rupture velocity exceeded the shear wave velocity of the Earth's crust north of San Francisco. Theoretical studies indicate that in-plane rupture can propagate at inter-sonic speeds (Burridge, 1973; Andrews, 1976). Other recent large strike-slip earthquakes: the 1999 Izmit; the 2001 Kunlunshan; and the 2002 Denali events, all exhibited super-shear rupture (Bouchon *et al*., 2001; Bouchon and Vallée, 2003; Dunham and Archuleta, 2004; Ellsworth *et al*., 2004). Recent lab experiments (Rosakis *et al*., 1999; Xia *et al*., 2004) confirm and extend previous work on super-shear rupture. Thus it seems plausible that super-shear rupture occurred during the 1906 San Francisco earthquake.

Geodetic Analysis

The differences between existing models of the earthquake are primarily north of Point Arena, where the San Andreas Fault runs offshore. 4.9 meters of slip was measured at Alder Creek, the northernmost observation of unambiguous faulting in the 1906 earthquake (Lawson, 1908). The same report found offset at Seal Cove, farther to the north, where the fault comes on shore again, but raised the possibility that this offset might have been due to landslides rather than faulting.

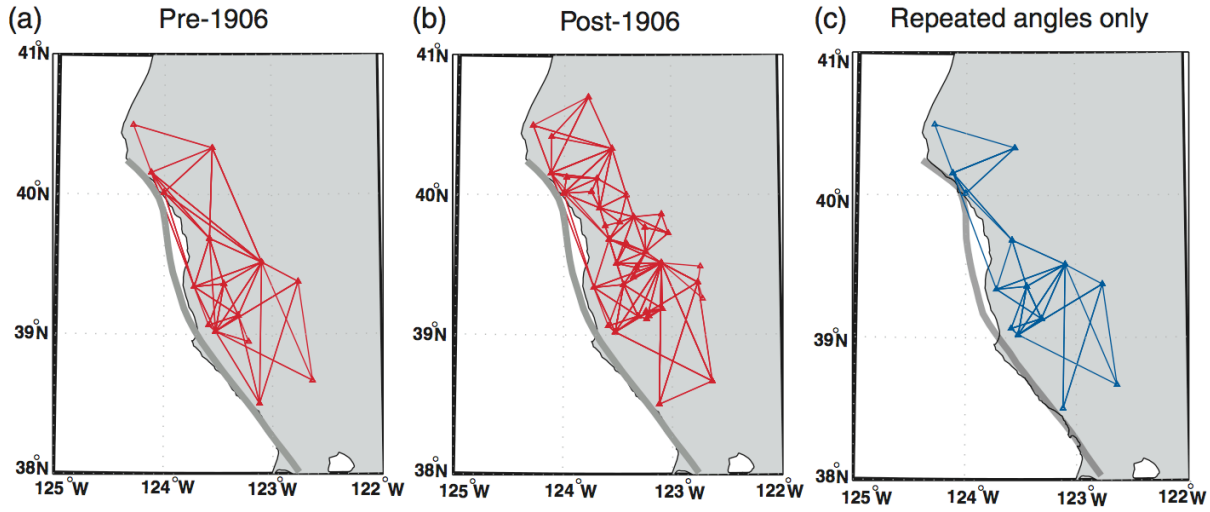

Figure 1. Triangulation network in the northern region of the San Andreas Fault used in the inversion before (a) and after (b) the 1906 San Francisco earthquake compared with network (c) of repeated angles only (Thatcher *et al*., 1997). The fault trace used in the study (Jachens *et al*., 2006) is shown as a thick solid line in (a) and (b). The solid line in (c) shows a fault trace used in the previous study. The time spans of the triangulation surveys before and after the earthquake are 1878-1892 and 1925-1942, respectively. An average standard deviation in angle measurement errors is less than 1 arc-sec for the post 1906 data set and about two arc-seconds for the pre 1906 data.

Thatcher *et al*. (1997), only used repeated measurements, which results in a weakly connected network north of Point Arena (Figure 1) and hence large uncertainties in the inferred slip. We use all available triangulation measurements in the northern region, employing a projection method to remove the dependence on initial station positions (Yu and Segall, 1996), which allows us to strengthen this part of the network. Our data in this region contains 60 pre-1906 and 172 post-1906 angle observations, compared with the 37 angle changes used previously.

The geodetic displacements along the entire rupture trace of the 1906 earthquake were estimated (Figures 2 and 3) using a model coordinate solution (Segall and Matthews, 1988). The result shows a displacement field characteristic of the co-seismic faulting as far north as Cape Mendocino. Two stations near the fault trace immediately south of Cape Mendocino show large displacements parallel to the local fault strike, which supports fault slip as opposed to land-sliding in this area. The magnitude of these vectors indicates that the slip was large.

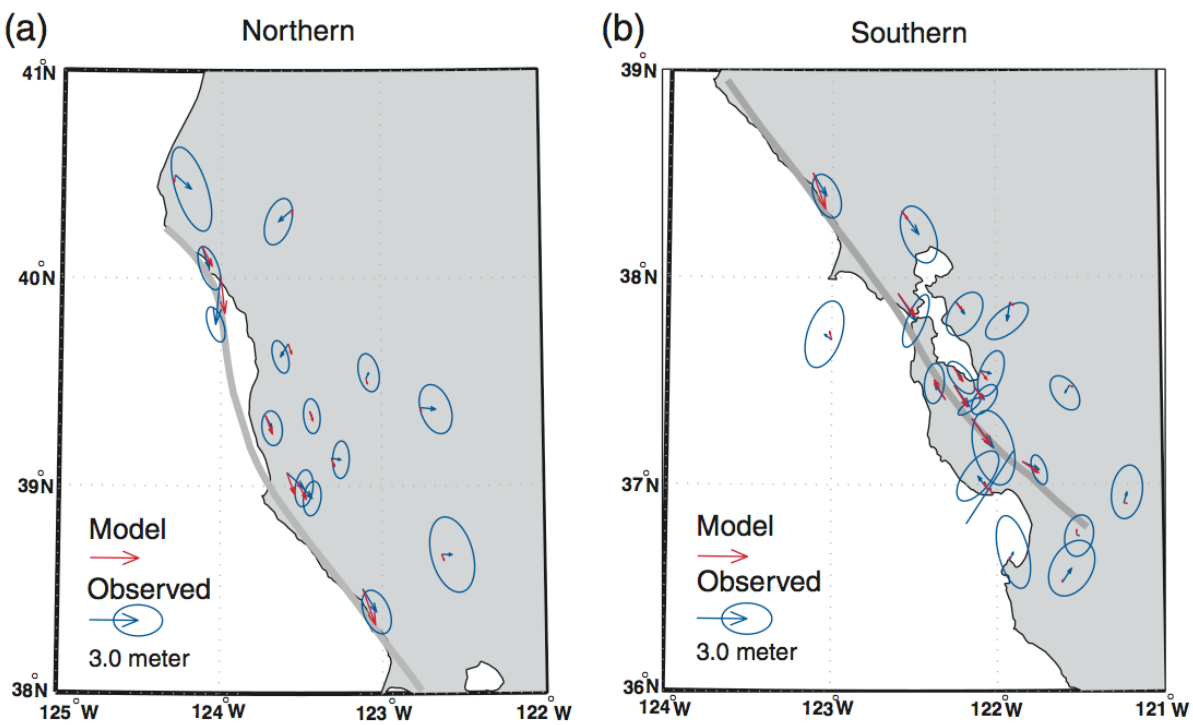

Figure 2. Estimated model coordinate displacement fields (blue arrows) with 95% confidence ellipses in the northern (a) and southern (b) region of the 1906 rupture. Predicted displacements are shown as red arrows, respectively. Stations near the fault in the northern region (a) show large displacements parallel to the local fault strike.

We estimate the co-seismic slip (Figure 4) by a linear inversion of the triangulation data with a fault trace obtained by Jachens *et al*. (2006). We assumed an elastic half-space, with each value representing average slip on 10 km long and 12 km wide (deep) vertical fault patch. The fault is assumed to be vertical. The average slip on each patch trades off with the vertical extent of the fault, which means that models with greater depth extent but smaller average slip could fit the data equally well. The integral of slip in the vertical direction, and hence the earthquake moment,

should not change much regardless of the rupture width. The slip distribution south of Point Arena is constrained only by the same repeated angle observations used in the previous study (Thatcher *et al*., 1997). The slip north of Point Arena is significantly improved by the use of non-repeated angles. Our slip on a ~500 km long rupture successfully fits the triangulation data, both confirming and refining the previous geodetic analysis (Thatcher *et al*., 1997).

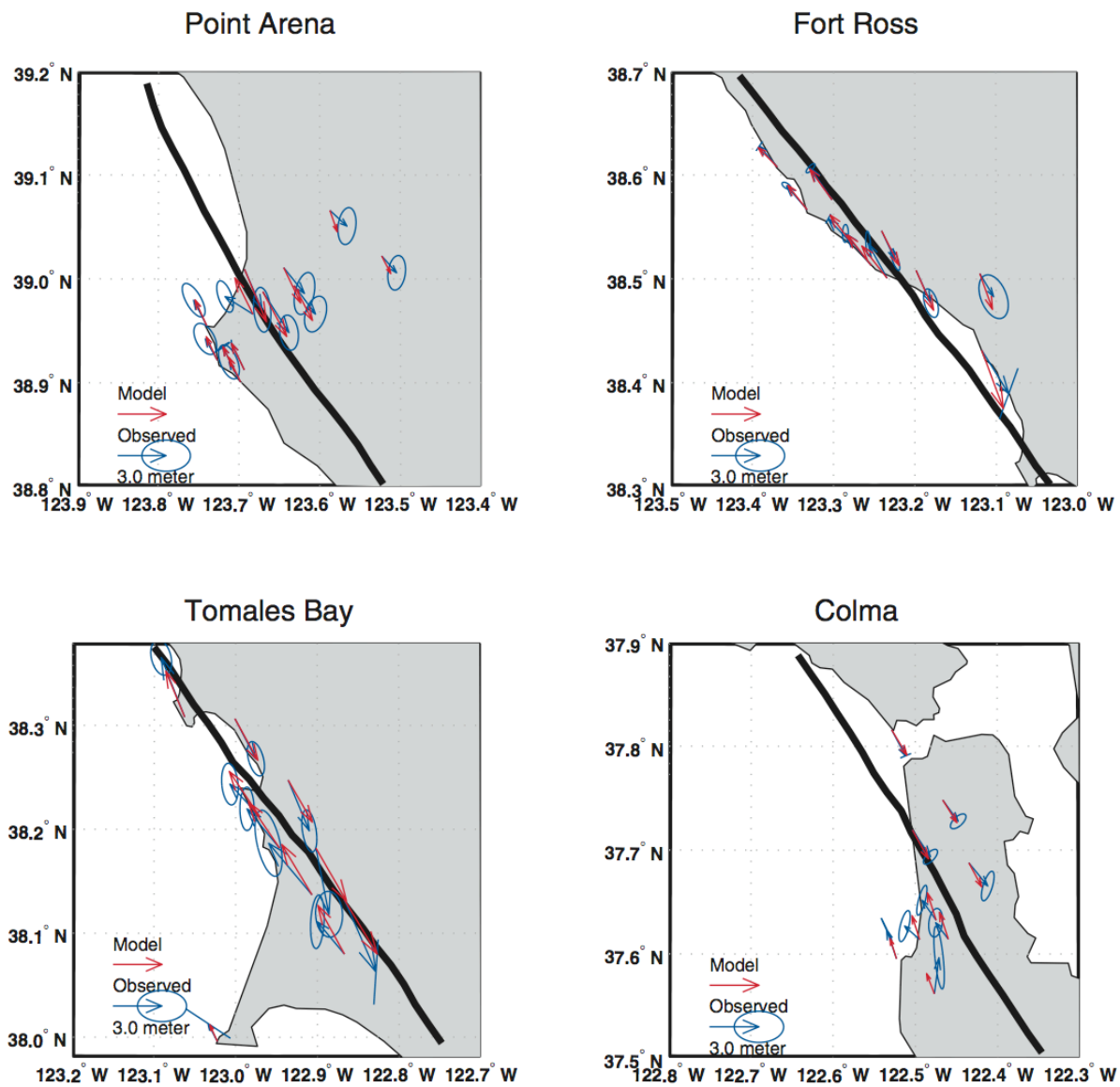

Fig. 3. Same as Figure 2, the estimated model coordinate displacement fields (blue arrows) with 95 % confidence ellipses in four local networks; (a) Point Arena, (b) Fort Ross, (c) Tomales Bay, (d) Colma.

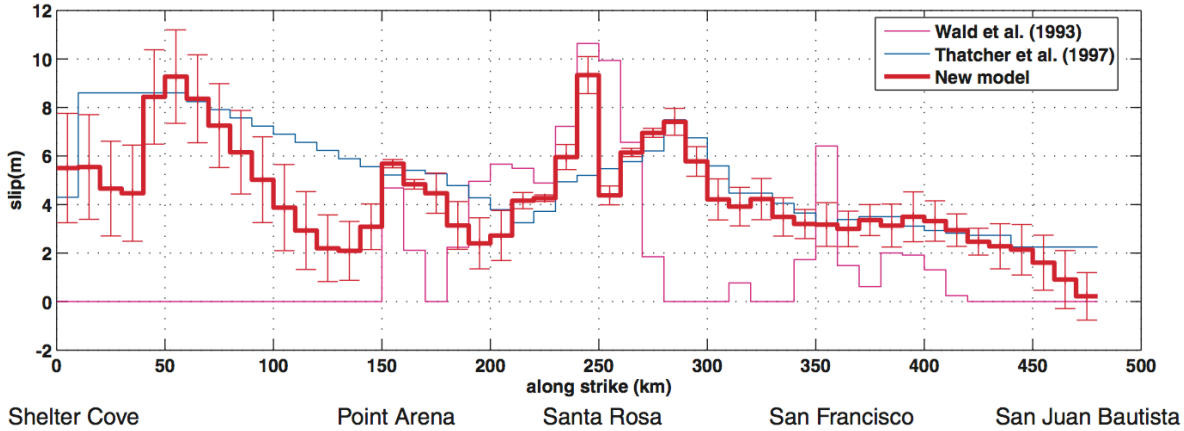

Fig. 4. Slip from inversion of geodetic data only, with 2 sigma errors. The previous slip models are shown for comparison (Thatcher *et al*., 1997; Wald *et al*., 1993). Slip varies only in the horizontal direction. Slip in the north is strongly constrained only by two nearby stations, resulting in relatively large errors. Larger errors notwithstanding, these results support large slip in this region. Slip in the southern region is similar to the previously obtained geodetic model because we used the same data set in that region. We did, however, find large slip between Fort Ross and Tomales Bay that was smoothed in the previous model of Thatcher *et al*. (1997).

Seismic Analysis

For long strike-slip events like the 1906 San Francisco earthquake, the duration of observed waveforms is constrained by the ratio of rupture length to rupture velocity. The duration of the observed teleseismic waves and the fixed 2.7 km/sec sub-Rayleigh rupture velocity assumed previously (Wald *et al*., 1993), favors a shorter fault rupture. Our hypothesis is that by allowing more flexibility in the rupture velocity, including the potential for super-shear rupture, we might fit all data with a single model.

The earthquake was recorded by over 90 seismographs worldwide and both seismograms and background information are well preserved (Reid, 1910). Data quality reflects the fact that these were the early days of instrumental seismology, and most records are not useful for waveform inversion. We used 5 stations, 8 components in total, including: two Wiechert Pendulum records from Europe, two Omori records from Japan, and one Bosch-Omori record from Puerto Rico. Those 5 stations were selected based on the proximity of observed Green's functions to the 1906 records and the need for azimuthal coverage.

We apply a Bayesian inversion approach, coupled with a Monte Carlo sampling method (Mosegaard and Tarantola, 2002; Metropolis *et al*., 1953). The posterior distribution of the model (slip and rupture velocity) is proportional to the product of a prior distribution and a likelihood function. The likelihood function contains only the seismic data. The geodetic results obtained above were used in the prior in order to stabilize the slip in the inversion. The prior for rupture velocity is a Gaussian distribution centered at the a sub-Rayleigh velocity (2.7 km/sec) with a 0.5 km/sec standard deviation. By assuming sub-shear rupture velocity in the prior, we ensure that the method will only find super-shear rupture if the data require it.

We use waveforms from the 1984 Morgan Hill earthquake as empirical Green's functions (Wald *et al*., 1993). Both the Morgan Hill and the San Francisco earthquake are vertical strike-slip events and share a similar strike, though the San Andreas bends in the northern and southern portion of the study area (Figure 2). The Green's function is time-lagged with rupture time along the fault. A linear summation of the time-lagged Green's function weighted by slip generates synthetic waveforms for the 1906 earthquake. The temporal evolution of slip on the fault is well beyond the resolving power of the data. Forward modeling indicates that the duration and amplitude of the teleseismic waves can constrain the duration of the rupture, and hence the average rupture velocity, when combined with the fault length determined from geodetic data.

Super-shear Rupture and a Combined Slip Model

Several locations have been suggested for the hypocenter of the earthquake by analyzing local and teleseismic observations (Reid, 1910; Bolt, 1968; Lomax, 2005). We used the latest estimate determined by A. Lomax (2005), which is located about 3 km west of the San Francisco zoo.

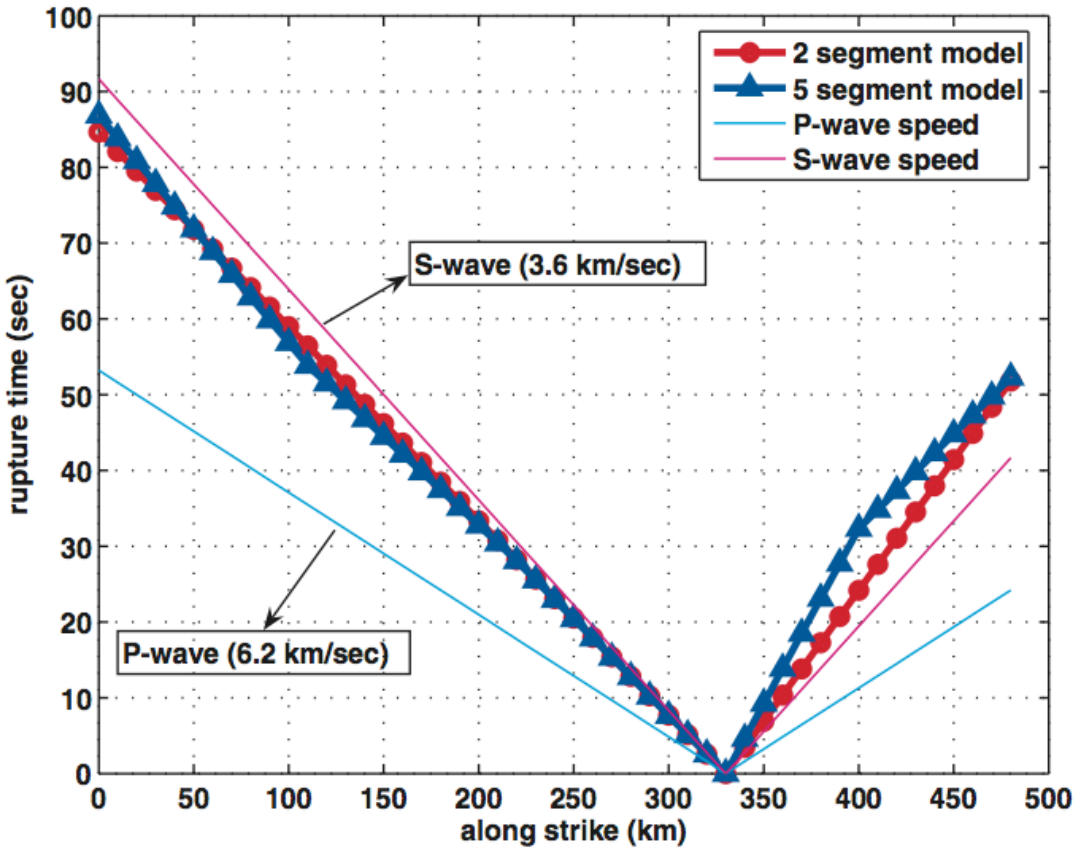

Fig. 5. Final slip models with 2 sigma errors obtained from both geodetic and seismic data compared with two previous slip models. Significant slip is observed in the northern region of the fault although the actual amount of slip is somewhat smaller than the previous geodetic slip (Thatcher *et al*., 1997). The rest is the same as Figure 4.

Rupture north of the hypocenter is constrained by the Gottingen and Uppsala seismogram, while rupture to the south is constrained by the Puerto Rico data. We find that it takes about 85 and 52 seconds, respectively, for the rupture to propagate along the northern (330 km long) and southern (150 km) segment from the hypocenter, which indicates that the rupture travels to the north at an average speed of 3.9 +/- 0.1 km/sec, exceeding the average shear wave velocity, and to the south at 2.9 +/- 0.1 km/sec, respectively. The formal errors of the rupture velocity estimates are small, due to the fact that neighboring points in seismic waveforms are correlated. In an attempt to localize the rupture velocity, we divided the rupture into five segments (3 segments north of the hypocenter, 110 km for each; 2 segments to the south, 70 and 80 km for each). While it is possible that the data could resolve such spatial variations in rupture velocity, the fact that the total rupture durations north and south of the hypocenter are about the same in both the two and five segment models (Fig. 5) suggests that while super-shear rupture to the north of the hypocenter is required to fit the data, it may be difficult to localize it further.

Figures 6 and 7 show the slip and waveform comparisons obtained from the two-segment model. Slip in the northern segment is smoother than that obtained from geodetic data (Fig. 4), but there is significant slip in the northern region. This confirms the long rupture length (~500 km) is compatible with the seismic data, though the amount of slip is smaller than the geodetically preferred value. The envelopes capture the duration and amplitude of the seismograms. The polarity of the synthetic waveform (SV component) at the PTR station is reversed, which can occur while fitting the waveform envelope. Inaccurate time alignment, an inaccurate Green's function, reversed polarity on the instrument, and delayed rupture to the southeast are all possible explanations of this mismatch. Because the fit at PTR is controlled by the slip and rupture propagation to the southeast of the hypocenter, it does not affect the inference that the rupture extended 500 km nor that rupture to the north of the hypocenter was super-shear.

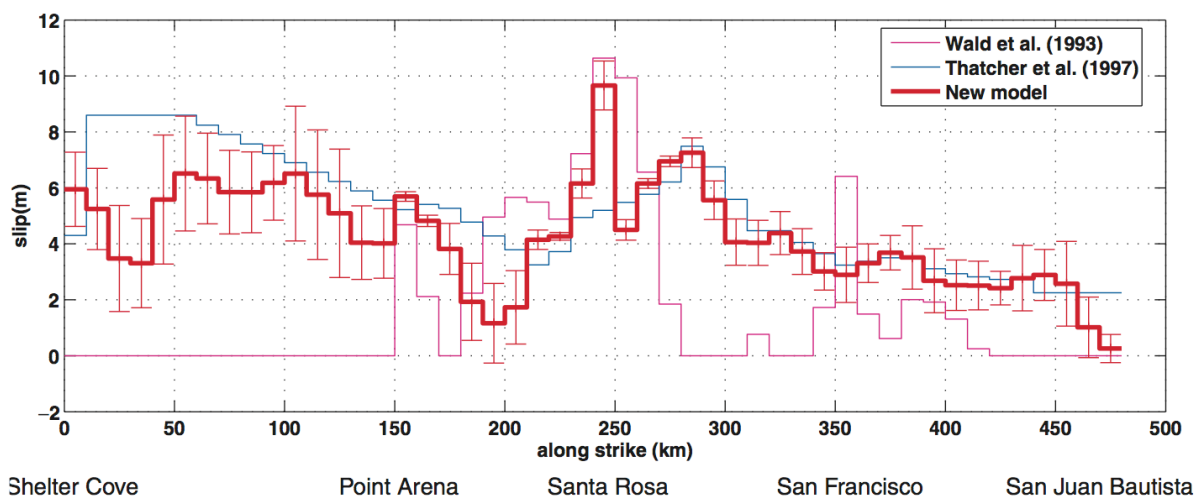

Fig. 6. Same as Figure 4, but for the combined model.

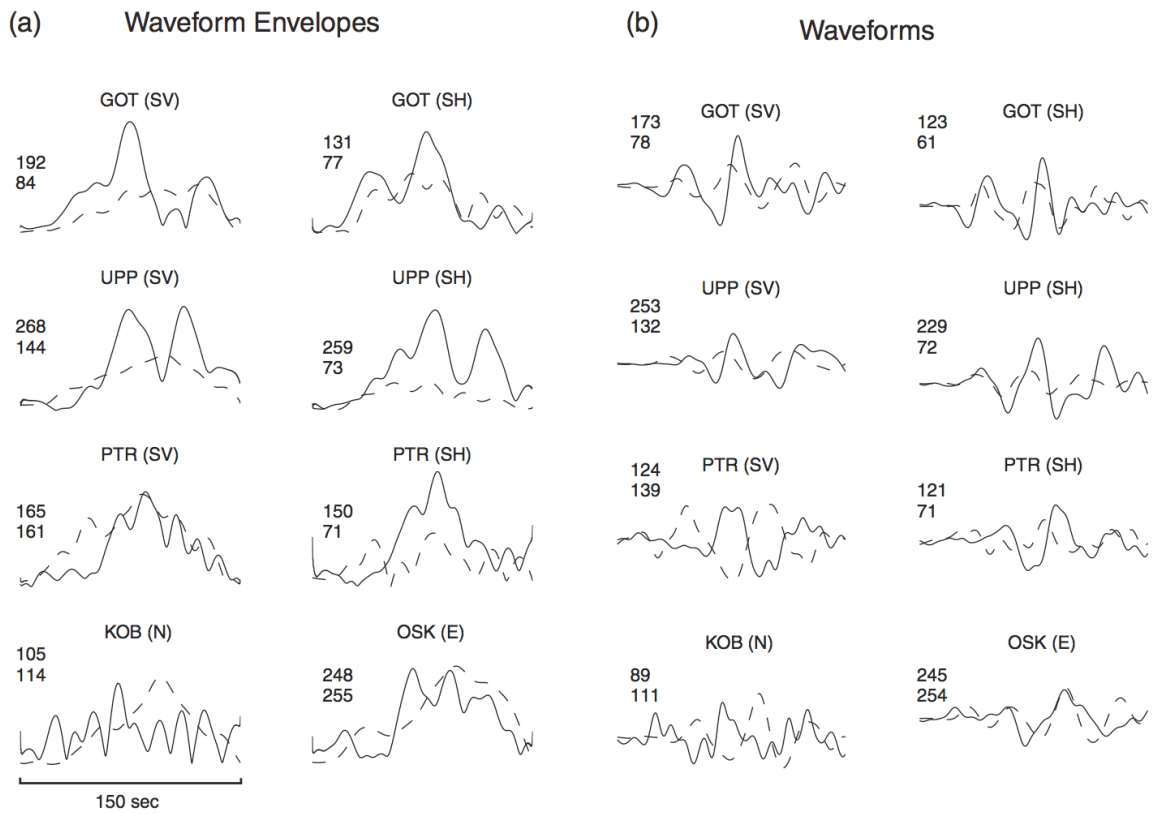

Fig. 7. Comparison of observed (solid) and calculated (dashed) waveforms and envelopes. Data are direct S-phases band-pass filtered between 0.01 and 0.1 Hz. Maximum amplitudes are given on the left of each trace in mm at the WWSSN LP seismograph (top: observed, bottom: calculated). Calculated waveform envelopes reproduce most of the amplitude and duration information of the observed waveform envelopes. Some stations also achieve good waveform fits, although our objective function is based on the envelopes (GOT: Gottingen, Germany, UPP: Uppsala, Sweden, PTR: Puerto Rico, W.I., KOB: Kobe, Japan, OSK: Osaka, Japan).

Our slip model has an average slip of 4.3 meters and a seismic moment of 7.9×10^{20} N-m, which corresponds to a moment magnitude of 7.9. Although the slip model was obtained by a joint inversion of the geodetic and seismic data, the slip distribution is primarily constrained by the triangulation data. Because the triangulation survey data used in this study span an interval as long as a 40 years, our slip estimates include postseismic and interseismic, as well as coseismic deformation. Long-term aseismic strain accumulates in the opposite direction of the deformation caused by earthquakes, which means that our estimate of M_w 7.9 should be considered a lower bound on the size of the 1906 earthquake.

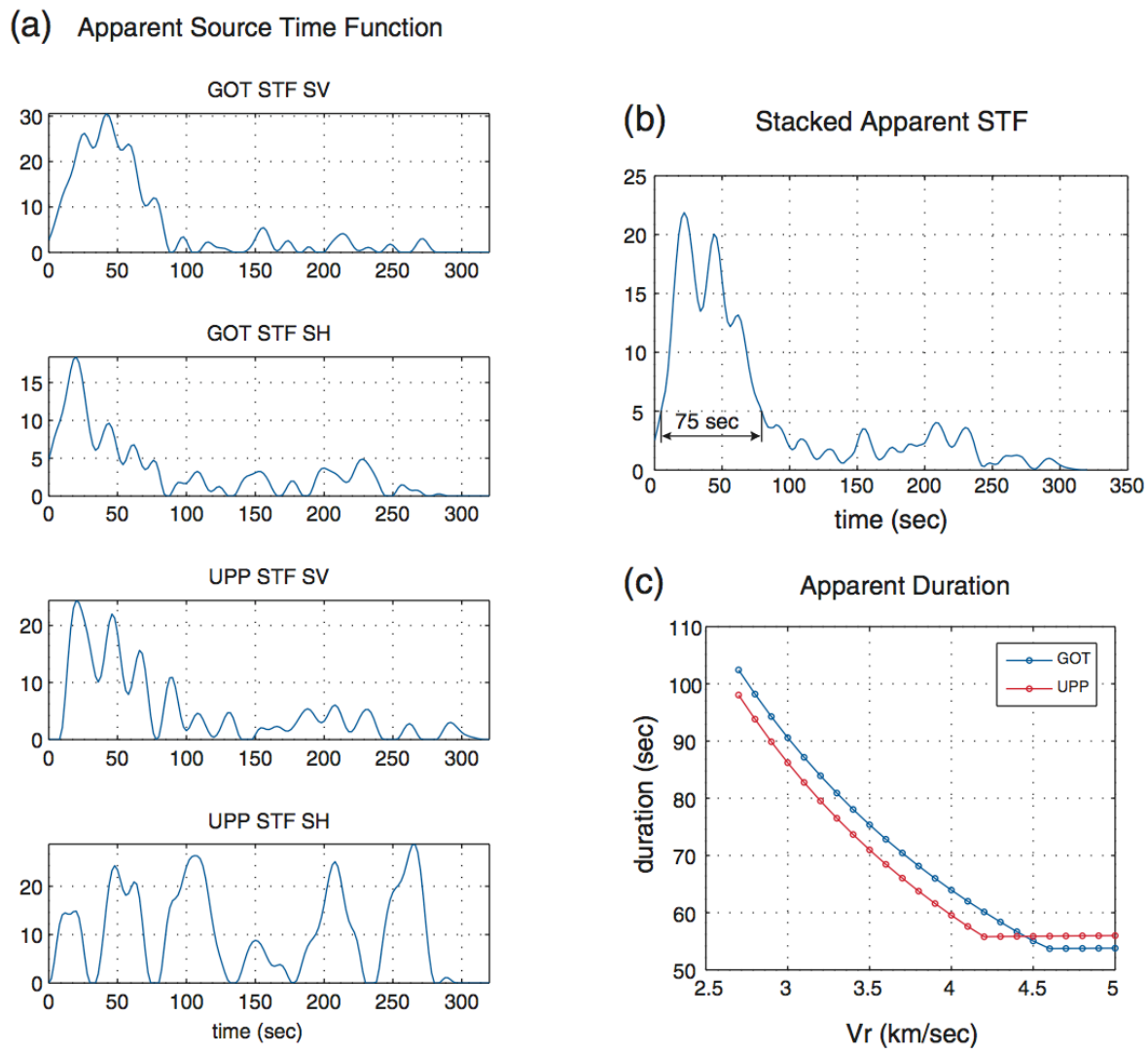

Fig. 8. Rupture duration of the earthquake inferred from the deconvolution of observed waveforms; (a) Apparent source time functions for two European stations (GOT and UPP), obtained from deconvolving the empirical Green's functions of the Morgan Hill earthquake from the observed waveforms. (b) Stacked version of the all source time functions except the SH component of the Uppsala station. (c) Expected duration of waveforms at each station as a function of the rupture velocity north of the hypocenter. Rupture velocity south of the hypocenter was fixed as 2.9 km/sec. Expected duration of waveforms were calculated from the maximum difference of arrival times from each fault patch. Duration of the apparent source time functions are well defined at each component except for the Uppsala SH, and is quite well resolved in the stacked source time function (b). Apparent rupture duration at the two European stations is about 75 seconds which is equivalent to a 3.4 km/sec average rupture velocity north of the hypocenter. This independent measure of the rupture duration of the earthquake supports the high rupture velocity, although the estimated velocity is less than in the kinematic inversion.

Discussion and Implications

The long rupture length is supported by intensity data from the 1906 earthquake (Boatwright and Bundock, 2005). The intensity map shows the severely damaged area (intensity VII or larger) extending north to the Mendocino triple junction and rules out the possibility that the slip on the fault north of Point Arena occurred aseismically. Moreover, a recent examination of the northernmost San Andreas Fault near Shelter Cove concluded that slip mapped there in 1906 was likely tectonic, extensive, and located on the main trace of the fault (Prentice *et al*., 1999).

Deconvolution of the empirical Green's functions from the 1906 seismograms yields an estimate of the apparent source duration and, given the fault length, the average rupture velocity. Using the European stations and employing positivity, smoothness, and moment-minimization constraints in a time domain deconvolution of the empirical Green's function event from the 1906 mainshock, we find a duration of ~ 75 seconds, which corresponds to an average rupture velocity of ~3.4 km/sec north of the hypocenter. This should be regarded as a lower bound since the smoothness constraint on the source time function deconvolution results in a longer duration, and hence lower inferred rupture velocity.

Both the intensity and the deconvolution support our long rupture length slip model with super-shear rupture. If the rupture velocity in this earthquake were super-shear, as we have suggested, then it has important implications for seismic hazard. First it demonstrates that slip models derived from geodetic and seismic observations are compatible, which is important for northern California because it provides a unified slip model to be used in recurrence models. Because the nature of strong ground motion for super-shear rupture is markedly different (Aagaard and Heaton, 2004), it will be necessary to account for this when predicting the level and the variability of strong ground motion in future large earthquakes.

References

Aagaard, B. T., and T. H. Heaton (2004). Near-source ground motions from simulations of sustained intersonic and supersonic fault ruptures, *Bull. Seism. Soc. Am.* **94**, 2064-2078.

Andrews, D. J. (1976). Rupture velocity of plane strain shear cracks, *J. Geophys. Res.* **81**, 5679-5687.

Boatwright, J., and H. Bundock (2005). Modified Mercalli Intensity maps for the 1906 San Francisco earthquake plotted in shake-map format, *U. S. Geol. Surv. Open-File Rept.* 2005-1135.

Bolt, B. A. (1968). The focus of the 1906 California earthquake, *Bull. Seism. Soc. Am.* **58**, 457-471.

Bouchon, M., M. P. Bouin, H. Karabulut, M. N. Toksöz, M. Dietrich, and A. Rosakis (2001). How fast is rupture during an earthquake? New insights from the 1999 Turkey earthquakes, *Geophys. Res. Lett.* **28**, 2723-2726.

Bouchon, M., and M. Vallée (2003). Observation of long supershear rupture during the magnitude 8.1 Kunlunshan earthquake, *Science* **301**, 824-826.

Burridge, R. (1973). Admissible speeds for plane-strain shear cracks with friction but lacking cohesion, *Geophys. J. R. Astr. Soc.* **35**, 439-455.

Dunham, E. M., and R. J. Archuleta (2004). Evidence for a supershear transient during the 2002 Denali fault earthquake, *Bull. Seism. Soc. Am.* **94**, S256-S268.

Ellsworth, W.L., M. Celebi, J.R. Evans, E.G. Jensen, R. Kayen, M.C. Metz, D.J. Nyman, J.W. Roddick, P. Spudich, C.D. Stephens (2004). Near-field ground motion of the 2002 Denali fault, Alaska, earthquake recorded at Pump Station 10, *Earthquake Spectra*, **20**, 597-615.

Jachens, R., R. Simpson, R. Graymer, C. Wentworth, and T. Brocher (2006). Three-dimensional geologic map of northern and central California: A basic model for supporting earthquake simulations and other predictive modeling, *Seism. Res. Lett.* **77**, 270-271.

Lawson, A. C. (1908). The California earthquake of April 18, 1906, Report of the State Earthquake Investigation Commission, Vol. 1, A. C. Lawson, Chairman, Carnegie Inst. of Washington, Washington, D. C. (reprinted 1969).

Lomax, A. (2005). A reanalysis of the hypocentral location and related observations for the great 1906 California earthquake, *Bull. Seism. Soc. Am.* **95**, 861-877.

Matthews, M. V., and P. Segall (1993). Statistical inversion of crustal deformation data and estimation of the depth distribution of slip in the 1906 earthquake, *J. Geophys. Res.* **98**, 12,153-12,163.

Metropolis, N., A. W. Rosenbluth, M. N. Rosenbluth, A. H. Teller, and E. Teller (1953). Equation of state calculations by fast computing machines, *J. Chem. Phys*. **21**, 1087-1092.

Mosegaard, K, and A. Tarantola (2002). Probabilistic approach to inverse problems, in *International Handbook of Earthquake & Engineering Seismology*, Part A., edited by W. H. K. Lee *et al*., pp. 237-265, Academic Press, San Diego, California.

Prentice C. S., D. J. Merritts, E. C. Beutner, P. Bodin, A. Schill, and J. R. Muller (1999). Northern San Andreas fault near Shelter Cove, California, *Geol. Soc. Am. Bull.* **111**, 512-523.

Reid, H. F. (1910). *The mechanics of the earthquake*, The California earthquake of April 18, 1906, Report of the State Earthquake Investigation Commission, Vol. 2, A. C. Lawson, Chairman, Carnegie Inst. of Washington, Washington, D. C. (reprinted 1969).

Rosakis, A. J., O. Samudrala, and D. Coker (1999). Cracks faster than the shear wave speed, *Science* **284**, 1337-1340.

Segall, P., and M.V. Matthews (1988). Displacement calculations from geodetic data and the testing of geophysical deformation models, *J. Geophys. Res.* **93**, 14,954-14,966.

Stein, S., and E. A. Okal (2005). Speed and size of the Sumatra earthquake, *Nature* **434**, 581 – 582.

Thatcher, W., G. Marshall, and M. Lisowski (1997). Resolution of fault slip along the 470-km-long rupture of the great 1906 San Francisco earthquake and its implications, *J. Geophys. Res.* **102**, 5353-5367.

Wald, D. J., H. Kanamori, D. V. Helmberger, and T. H. Heaton (1993). Source study of the 1906 San Francisco earthquake, *Bull. Seism. Soc. Am.* **83**, 981-1019.

Xia, K., A. J. Rosakis, and H. Kanamori (2004). Laboratory earthquakes:the sub-Rayleigh-to-supershear transition, *Science* **303**, 1859-1861.

Yu, E., and P. Segall (1996). Slip in the 1868 Hayward earthquake from the analysis of historical triangulation data, *J. Geophys. Res.* **101**, 16,101-16,118.